Original Article

MOLECULAR METABOLISM

The MicroRNA *miR–696* is regulated by SNARK and reduces mitochondrial activity in mouse skeletal muscle through Pgc1α inhibition

André L. Queiroz [1,2], Sarah J. Lessard [2], Amanda T. Ouchida [1], Hygor N. Araujo [3], Dawit A. Gonçalves [1], Dimitrius Santiago P. Simões Fróes Guimarães [3], Bruno G. Teodoro [1,4], Kawai So [2], Enilza M. Espreafico [5], Michael F. Hirshman [2], Luciane C. Alberici [4], Isis do Carmo Kettelhut [1], Laurie J. Goodyear [2,], Leonardo R. Silveira [3,*]**

ABSTRACT

Objective: MicroRNAs (miRNA) are known to regulate the expression of genes involved in several physiological processes including metabolism, mitochondrial biogenesis, proliferation, differentiation, and cell death.
Methods: Using "in silico" analyses, we identified 219 unique miRNAs that potentially bind to the 3′UTR region of a critical mitochondrial regulator, the peroxisome proliferator-activated receptor gamma coactivator (PGC) 1 alpha (*Pgc1α*). Of the 219 candidate miRNAs, *miR-696* had one of the highest interactions at the 3′UTR of *Pgc1α*, suggesting that *miR-696* may be involved in the regulation of *Pgc1α*.
Results: Consistent with this hypothesis, we found that *miR-696* was highly expressed in the skeletal muscle of STZ-induced diabetic mice and chronic high-fat-fed mice. C2C12 muscle cells exposed to palmitic acid also exhibited a higher expression of *miR-696*. This increased expression corresponded with a reduced expression of oxidative metabolism genes and reduced mitochondrial respiration. Importantly, reducing *miR-696* reversed decreases in mitochondrial activity in response to palmitic acid. Using C2C12 cells treated with the AMP-activated protein kinase (AMPK) activator AICAR and skeletal muscle from AMPKα2 dominant-negative (DN) mice, we found that the signaling mechanism regulating *miR-696* did not involve AMPK. In contrast, overexpression of SNF1-AMPK-related kinase (SNARK) in C2C12 cells increased *miR-696* transcription while knockdown of SNARK significantly decreased *miR-696*. Moreover, muscle-specific transgenic mice overexpressing SNARK exhibited a lower expression of *Pgc1α*, elevated levels of *miR-696*, and reduced amounts of spontaneous activity.
Conclusions: Our findings demonstrate that metabolic stress increases *miR-696* expression in skeletal muscle cells, which in turn inhibits *Pgc1α*, reducing mitochondrial function. SNARK plays a role in this process as a metabolic stress signaling molecule inducing the expression of *miR-696*.

Keywords *miR-696*; Mitochondrial function; Skeletal muscle; SNARK; *Pgc1α*

1. INTRODUCTION

Metabolic syndrome is a systemic disorder associated with several pathological conditions including type 2 diabetes, obesity, hypertension, glucose intolerance, insulin resistance, and dyslipidemia. There is evidence that mitochondrial dysfunction and alterations in the expression of metabolic genes correlate with these diseases [1,2]. Increased inflammatory processes and defects in fatty acid or glucose metabolism have also been linked to diet-induced obesity and the development of insulin resistance in several tissues including skeletal muscle [3], liver [4], and adipose tissue [5].

It is widely accepted that the peroxisome proliferator-activated receptor gamma coactivator-1α (*Pgc1α*) regulates mitochondrial biogenesis in skeletal muscle through coactivation of the nuclear receptors PPARβ, ERRα, and thyroid hormone receptor and nuclear respiratory factors NRF1 and NRF2 [6—8]. For example, NRF1 and 2 induce transcription factor A, mitochondrial (TFAM), leading to the transcription of several mitochondrial DNA genes [9]. Therefore, *Pgc1α* is a critical regulator of mitochondrial biogenesis, oxidative metabolism, fiber-type switching, fatty acid oxidation, and angiogenesis [10—12]. *Pgc1α* transcription is regulated by an alternative splicing mechanism, resulting in four unique isoforms: *Pgc1α*-1, α-2, α-3, and α-4 [13]. *Pgc1α* is also regulated by post-translational modifications

[1]Department of Biochemistry and Immunology, Ribeirão Preto Medical School, USP, Ribeirão Preto, Brazil [2]Research Division, Joslin Diabetes Center, and Department of Medicine, Brigham and Women's Hospital and Harvard Medical School, Boston, MA, USA [3]Obesity and Comorbidities Research Center, OCRC, IB, UNICAMP, Campinas, Brazil [4]Department of Physics and Chemistry, Faculty of Pharmaceutical Science, USP, Ribeirão Preto, Brazil [5]Department of Cell Biology, Ribeirão Preto Medical School, USP, Ribeirão Preto, Brazil

*Corresponding author. E-mail: leors@unicamp.br (L.R. Silveira).

**Corresponding author. E-mail: Laurie.Goodyear@joslin.harvard.edu (L.J. Goodyear).

Received January 13, 2021 • Revision received March 16, 2021 • Accepted March 25, 2021 • Available online 31 March 2021

https://doi.org/10.1016/j.molmet.2021.101226

involving 5′ AMP-activated protein kinase (AMPK) [14] and sirtuin 1 (SIRT1) [15].

Another level of *Pgc1α* regulation may be through microRNAs, small non-coding RNA molecules that disrupt post-transcriptional processes by impairing protein translation [16]. As examples, microRNA *miR-23a* was shown to downregulate *Pgc1α* and was ascribed as a major cause of mitochondrial dysfunction in estrogen-deficient mice [17], whereas *miR-761* was reported to be involved in the biogenesis of mitochondria through the downregulation of *Pgc1α* [18]. *miR-696* was first reported to be expressed in prenatal development (E9.5) of mouse embryos at an intergenic loci on chromosome 3 (mm10, 30852687-30852704) [19]. *miR-696* was shown to be decreased by exercise training and increased by hindlimb immobilization in skeletal muscles of wild-type mice [20]. Moreover, C2C12 muscle cells transfected with a *miR-696* mimic oligonucleotide markedly reduced mitochondrial DNA content and the ATP/ADP ratio, while *miR-696* antisense oligonucleotide (ASO) treatment decreased intracellular triacylglycerol content [21]. The potential roles of *miR-696* in regulating muscle metabolism under conditions of metabolic dysregulation such as insulin resistance and obesity have not been investigated.

AMPK activity increases in response to increase in AMP and ADP concentrations [22]. AMPK has been implicated in the regulation of a plethora of cellular effects including glucose uptake, fatty acid oxidation, and mitochondrial gene expression [23]. Decreased AMPK activity correlates with reduced *Pgc1α* expression and thus metabolic consequences including mitochondrial dysfunction [14,24]. In addition to AMPK, there is a family of AMPK-related kinases with different cellular functions that share the same upstream kinase in LKB1 [25] such as sucrose non-fermenting-related kinase (SNRK), a protein involved in the metabolic properties of cardiac and adipose tissues [26—28] or SNF1-AMPK-related kinase (SNARK), whose expression has been reported to be increased under a variety of altered metabolic conditions including C2C12 cells exposed to palmitic acid and tumor necrosis factor alpha (TNFα), skeletal muscle of chronic high-fat-fed mice, and skeletal muscle from obese and older subjects [29,30]. Given that all of these stimuli provoke cellular stress, it is interesting that SNARK has been shown to function as a nuclear stress-response transcription modulator [31]. Herein, we used cell and in vivo mouse models to test the hypothesis that increased *miR-696* reduces mitochondrial function in skeletal muscle through the inhibition of Pgc1α. Furthermore, we determined the role of AMPK and the AMPK-related kinase SNARK in this signaling axis.

2. METHODS

2.1. Streptozotocin-treated (STZ) mice

C57BL/6J male mice (10—16 weeks old) were maintained on a 12:12-h light—dark cycle with ad libitum access to water and chow. To induce insulin-deficient diabetes, the mice were injected with streptozotocin (STZ, 70 mg kg^{-1}) through the jugular vein under isoflurane anesthesia. STZ was dissolved in 0.01 M of citrate buffer (pH 4.5). Control mice received only citrate buffer (vehicle) under the same conditions. The mice were sacrificed three days after STZ injection and blood glucose levels were determined by a glucometer. The tibialis anterior (TA) muscle was dissected from both groups, immediately frozen in liquid nitrogen, and stored at −80 °C. Biochemical blood parameters and body weights are available in the Supplementary material Table 1.

2.2. High-fat diet (HFD) mice

Six-week-old C57BL/6J mice were maintained on a 12:12-h light—dark cycle with ad libitum access to water and diet. HFD mice were fed a diet composed of 20% protein, 20% carbohydrate, and 60% fat (Research Diets; product data D12492) for 10 weeks to induce obesity. Control mice were fed a diet composed of 20% protein, 70% carbohydrate, and 10% fat (Research Diets; product data D12450B). The mice were sacrificed at 16 weeks of age and their TA and extensor digitorum longus (EDL) muscles were dissected for experimental analyses. Biochemical blood parameters and body weights are available in the Supplementary material Table 2.

2.3. Generation of AMPK and SNARK transgenic mice

Transgenic mice expressing AMPK with an inactivating D157A mutation in the α2 subunit (AMPKα2 DN) and transgenic mice expressing AMPK with an activating R70Q mutation in the γ1 subunit (AMPKγ1 R70Q) were generated on an FVB background as previously described [32,33]. Dominant-negative SNARK (SNARK DN) and overexpressing wild-type SNARK (SNARK WT) mice were generated on a C57BL/6 background as previously described [29]. Wild-type (WT) littermates were used as controls. The mice were sacrificed at 10—18 weeks of age and their TA muscles were dissected for experimental analyses.

2.4. Exercise capacity tes

Mice (5—7 males) were placed in treadmill lanes to perform maximal exercise capacity. Shocking grids with the frequency set at 75 per minute and intensity at 45% (3.4 mA) were placed at end of the treadmill to force the mice to run at their maximum. The protocol started with speed at 6 m/min followed by incremental adjustments of 2 m/min every 2 min until fatigue was reached. Fatigue was defined as the mouse being stationary on the shocking grid with no attempts to climb off for 20 s. The maximum speed, time, and laps were then recorded and used to calculate the total time, total distance, and work.

2.5. Indirect calorimetry

Mice were individually housed at 22 °C and subjected to indirect calorimetry (Comprehensive Laboratory Animal Monitoring System, CLAMS; Columbus Instruments) for a period of 3 consecutive days under a 12-h light—dark cycle. During this period, we measured their food and water intake, spontaneous activity, and volume of oxygen and carbon dioxide consumed. These data allowed us to estimate the total energy expenditure (TEE) and respiratory exchange ratio (RER). We recorded SDN and SWT mice in three phases: 1) Acclimation, first 24 h of measurement. 2) Fed, 24 h after the end of phase 1, the mice were fed ad libitum. 3) Fasted, 24 h after the end of phase 2, the mice were fasted during the period. Spontaneous activity was extrapolated from the real-time analysis of total mouse activity with a 0.25 cm calculated centroid (how much each mouse moved in the cage). The software analysis package provided a graphical representation of their position within the cage, calculated the total distance traveled, displayed rearing information, correlated activity and distance traveled, and stored the raw position vs time data for other traceable and quantifiable analyses of activity levels.

2.6. Plasmids and constructs

Full-length *Pgc1α* plasmid, GFP, and RFP reporter plasmids were purchased from Addgene (cat. #4, #35625, and #35626). Approximately 165 bp of mouse *Pgc1α* 3′UTR was synthesized from brown adipose tissue cDNA through PCR using AccuPrime Taq DNA polymerase and cloned into *Pgc1α* (*Pgc1α*-3′UTR), GFP (GFP-PGC1-3′UTR), and GFP (GFP-PGC1-3′UTRmt (mutation of two nucleotides in positions 4 and 5 at the seed region)) reporter plasmids with T4 ligase enzyme according to the manufacturer's instructions (New England Biolabs). *Pgc1α* 3′UTR was synthesized with a mutated site for *miR-696* interaction using AccuPrime Taq DNA polymerase and cloned into GFP (GFP-PGC1-3′UTRmt) reporter plasmid. The 3′ and 5′ *miR-696* oligonucleotide

sequences (Eurofins) with BspQ1 overhangs were annealed for 5 min at 95 °C, followed by 10 min at 4 °C. Then the annealing product was cloned into an RFP reporter (RFP-miR696) plasmid using a BspQ1 enzyme (New England Biolabs). SNARK plasmids were generated as previously described [29]. Constructs were sequenced by the DNA Sequencing Core Facility at Brigham and Women's Hospital.

2.7. Cell culture

To isolate and culture primary rat myocytes, cells were seeded in dishes covered with Matrigel (0.1%) until they reached maturity (5—6 days) at a density of 2.5×10^5 cells/well as previously described [30]. For C2C12 cells, approximately 2×10^5 myoblast cells were seeded and cultured in DMEM containing 10% FBS and 1% penicillin/streptomycin at 37 °C with 5% CO_2 for 2 days until they reached 90% of confluence. Differentiation was induced by incubating the cells in DMEM containing horse serum (2%) and penicillin/streptomycin (1%) for 4 days, and the medium was changed every 2 days. On day 5 of differentiation, the cells were incubated with AICAR (250 μM), palmitic acid (500 or 700 μM containing fatty acid-free BSA 1%), or vehicle (ethanol containing fatty acid-free BSA 1%) for 24 h. For HEK293 cells, 2×10^5 human embryonic kidney 293 (HEK293) cells were seeded and maintained in DMEM containing FBS (10%) and penicillin/streptomycin (1%) at 37 °C with 5% CO_2.

2.8. Plasmid, siRNA, miR, and anti-miR transfection

For rat myotube cell cultures, full-length *Pgc1α* plasmid was mixed with Lipofectamine 2000 in Opti-MEM medium according to the manufacturer's instructions (Life Technologies) and then added to the cell cultures on day 3 of differentiation (~60% confluence) and maintained at 37 °C with 5% CO_2. The cells were washed with DPBS, and then primary growth medium (PGM) containing FBS (10%), HS (10%), and penicillin/streptomycin (1%) was added 12 h after transfection. Experiments were performed on day 5 of differentiation. Control cells were transfected with pcDNA3 empty vector or GFP. Myoblasts from C2C12 cells were exposed to the reverse transfection protocol using full-length human SNARK plasmid conjugated to Viromer Red reagent in buffer E medium as recommended by the manufacturer (Lipocalyx). Twelve hours after transfection, the cells were washed with PBS and incubated with DMEM medium containing horse serum (2%). Experiments were performed 48 h after reverse transfection. Control cells were transfected with either pcDNA3 empty vector or GFP. For RNA transfection, C2C12 cells were transfected on day 3 of differentiation using Lipofectamine RNAiMAX reagent (Invitrogen-Life Technologies). siRNA against SNARK or scrambled sequences were obtained from Origene (SR30004, SR418439B). The *miR-696* mimic, *miR-696* ASO, and scrambled sequences were synthesized by miRIDIAN (Dharmacon-GE).

2.9. Reporter assay

HEK293 cells were transfected with GFP-3′UTR, GFP-3′UTRmt, RFP-miR696, or RFP-miR30 using Viromer Red reagent in buffer E medium (Lipocalyx). The medium was changed 24 h after transfection with 1 μg/mL of doxycycline in DMEM containing FBS (10%). After transfection for 72 h, the cells were fixed with paraformaldehyde (4%) and stained with 1 μg/mL of DAPI (Cat. No. D9564; Sigma-Aldrich). Images were obtained under 40× magnification on a fluorescence microscope (Zeiss) and quantified using ImageJ software.

2.10. Western blotting analysis

Protein samples isolated from C2C12 cells (30 μg) and rat primary myocyte-cultured cell lysates (100 μg) were separated by SDS-PAGE on an acrylamide gel (10%). Non-specific binding was blocked with fat-free milk (10%) for 60 min. The membranes were incubated overnight at 4 °C with primary antibodies: PGC-1alpha (Calbiochem, ST1202), p-Akt Ser^{473} (Cell Signaling, #9271), total Akt (Cell Signaling, #9272), total SNARK (anti-NUAK2 Abcam, ab107287), p-SNARK Thr^{208} (Cell Signaling), FLAG (Sigma-Aldrich, F7425), and β-actin (Santa Cruz, sc-47778). The membranes were incubated with HRP-conjugated secondary antibodies for 60 min at room temperature. Antibody binding was detected using Amersham ECL reagent (GE) as described by the manufacturer. Blots were scanned using a ChemiDoc imaging system (Bio Rad), and protein band densitometry was determined using ImageLab software (Bio-Rad).

2.11. Real-time quantitative PCR (qPCR)

Total RNA was isolated using TRIzol reagent (Invitrogen). One microgram of total RNA was used for complementary DNA synthesis performed using a high-capacity reverse-transcription kit (Applied Biosystems). For real-time PCR analysis, RNA was reverse transcribed using Power SYBR Green Master Mix (Applied Biosystems). The relative expression of mRNAs was determined after normalization using the ΔΔCt method. Quantitative PCR was performed using a StepOne Real-Time PCR System (Applied Biosystems). The sequence of all primers can be found in the Supplementary material. β-actin, GAPDH, or RPL39 were used as reference genes.

2.12. TaqMan MicroRNA qRT-PCR

Using a TaqMan miRNA reverse-transcription kit (Applied Biosystems), 7.5 μL of cDNA reaction products were produced from 5 ng of total RNA with specific stem-loop primers for mmu-*miR-696* and mmu-SnoR-202. The cDNA was then diluted (15×) and amplified using the TaqMan miRNA assay together with TaqMan Universal PCR Master Mix (Applied Biosystems) on an ABI Prism 7500 system (Applied Biosystems). The mmu-*miR-696* Ct range was between 29 and 34 and mmu-SnoR-202 between 25 and 27. The mmu-SnoR-202 was used as a reference. The miRNA expression was quantified by the ΔΔCt method.

2.13. Oxygen consumption in myotubes

C2C12 cells at a density of 1×10^6 were seeded in 100 mm culture plates. After treatment, the cells were trypsinized, centrifuged (1250 RPM), and incubated with 2 mL of air-saturated respiration medium in an Oxygraph-2k (O2k, OROBOROS Instruments). During measurements of oxygen consumption, oligomycin (1 μg/mL), an ATP synthase inhibitor, and carbonyl cyanide m-chlorophenylhydrazone (CCCP, 1 μM), a mitochondrial uncoupling activator, were used for oxidative phosphorylation inhibition and mitochondrial uncoupling, respectively.

2.14. Oxygen consumption in myoblasts

Cells at a density of 2×10^4/well were seeded in XF 24-well cell culture microplates in 350 μL of FBS (10%) medium and incubated at 37 °C with 5% CO_2. After 48 h, experiments were initiated in 675 μL of DMEM medium without phenol containing 1.85 g/L of NaCl, 2 mM of GlutaMax-1, 1 mM of sodium pyruvate, 15 mM of D-glucose, and 20 mM of HEPES at a pH of 7.4. The cells were incubated at 37 °C without CO_2 for 60 min before the first measurement. During oxygen consumption measurements, oligomycin (1 μg/mL), an ATP synthase inhibitor, carbonyl cyanide-p-trifluoromethoxyphenylhydrazone (FCCP, 1 μM), a mitochondrial uncoupling activator, and rotenone (0.1 μM), a mitochondrial complex I inhibitor, were added at various intervals. The Δ oxygen consumption rate (ΔOCR) was measured according to the following calculations: basal respiration = basal − rotenone; uncoupled respiration = oligomycin − rotenone; maximal respiration = FCCP − rotenone. Experiments were performed using an XF 24-well Seahorse (Seahorse Biosciences).

2.15. Determining ROS production

The cells were maintained at 37 °C in PBS containing glucose (5.6 mM), fluorescent Amplex UltraRed (50 μM), and horseradish peroxidase (HRP) (0.1 U/mL) for 60 min. The medium was collected and fluorescence intensity determined at 568 nm excitation and 581 nm emission. The cells were transfected with scramble oligo, *miR-696* mimic or anti-*miR-696* with palmitic acid (700 μM), or palmitic acid alone (700 μM). The antioxidants glutathione (GSH) and glutathione peroxidase were added as a negative control.

2.16. Tricarboxylic acid cycle intermediates (ICAT)

A total of 2×10^5 C2C12 cells were seeded in a 6-well plate. After treatment, the cells were collected with the addition of perchloric acid (0.5 M) containing EDTA (1 mM) and neutralized with $KHCO_3$ (2.2 M), then centrifuged at 7000 rpm for 10 min. The metabolites citrate, malate, oxaloacetate, and α-ketoglutarate were detected as previously described [64].

2.17. ATP content

ATP was measured in C2C12 cells exposed to either AICAR (250 μM) or palmitic acid (500 μM and 700 μM) using an ATP assay kit (Sigma-Aldrich, Cat. Number FLAA) according to the manufacturer's protocol.

2.18. Determining glucose uptake

Cells were incubated at 37 °C in DMEM with 2 mM of glucose without serum for 2—3 h. The media was changed to DPBS (1 mL) containing glucose (5.6 mM), insulin (100 nM), and 2-deoxy-[1,2-^{3}H]-glucose (0.1 μCi/mL). After 30 min, the cells were washed in DPBS and lysed in NaOH (0.1 N). Radioactivity was determined by liquid scintillation counting and 2-deoxyglucose uptake was calculated based on the DPM results divided per sample protein concentration.

2.19. In silico analysis

The raw data were collected through Sfold 2.2 online software (http://sfold.wadsworth.org/cgi-bin/index.pl). To acquire the raw data, we used the STarMirDB database prediction model training data (species: HITS-CLIP, mouse) to show the potential Ppargc1a binding microRNA candidates. Hybridization free energy (hΔG) was selected to rank the microRNAs listed. The data were plotted in Plotly online software (https://plotly.com/) to create the graph in Figure 1. A cut-off inferior to −20 kcal/mol was applied for illustrative purposes.

2.20. Study approval

SNARK experiments were performed in accordance with a protocol approved by the Joslin Diabetes Center Institutional Animal Care and Use Committee and were in accordance with the Guide for the Care

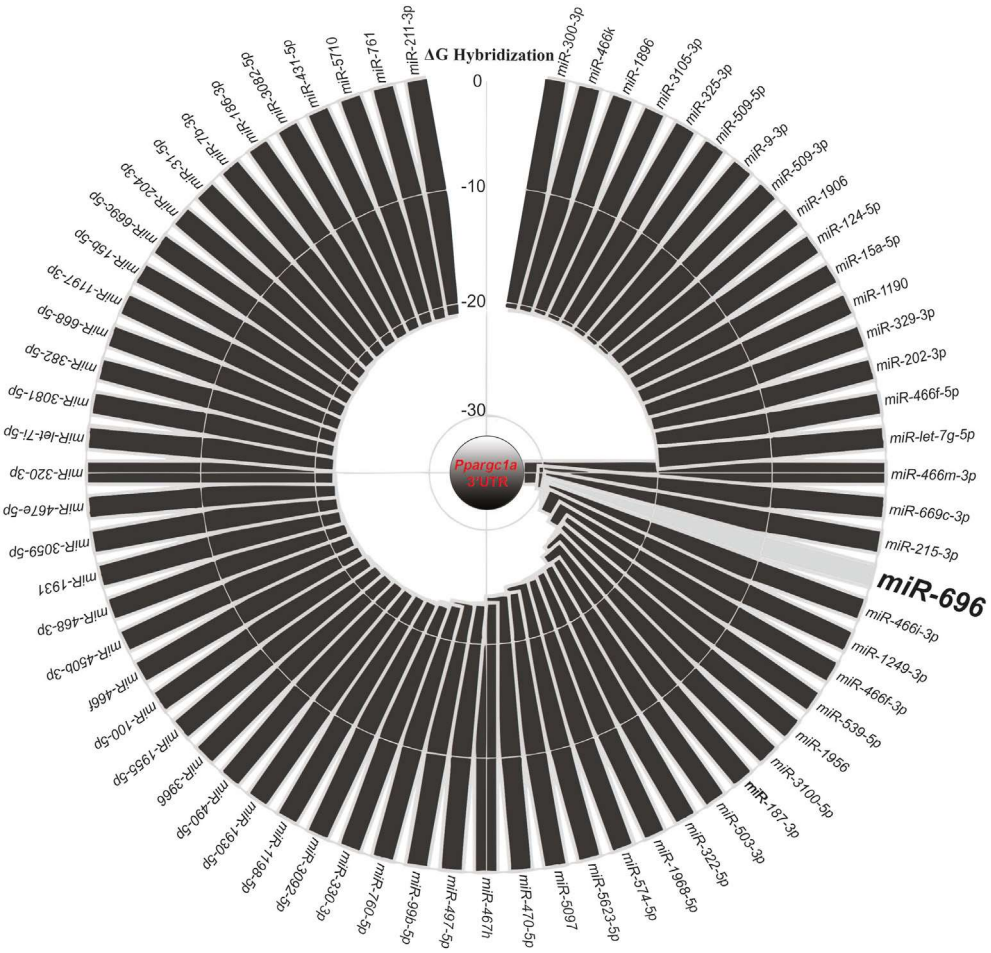

Figure 1: Database interaction analysis of *Pgc1α* gene and microRNAs. "In silico" bioinformatics analysis using Sfold 2.2 (http://sfold.wadsworth.org/cgi-bin/index.pl) was conducted to determine all reported *Mus musculus* microRNAs that bind to *Pgc1α* 3′UTR. Hybridization free energy (ΔG) indicates interactions between all listed microRNAs and *Pgc1α* 3′UTR. A cut-off inferior to −20 kcal/mol was applied for illustrative purposes.

and Use of Laboratory Animals (eighth edition, National Academies Press, 2011). Procedures for inducing diabetes by STZ and isolating rat cells were approved by the Institutional Ethical Committee for the use of laboratory animals from the University of Sao Paulo, Ribeirao Preto Campus (Approval Nos. 092/2010 and 130/2012).

2.21. Statistics

Results were expressed as a mean ± standard error of the mean (S.E.M) and analyzed by t tests or one-way ANOVA followed by Tukey's test for multiple comparisons. $p \leq 0.05$ was taken as the criterion for significance.

3. RESULTS

3.1. Database interaction analysis of Pgc1α gene and microRNAs

Reduced mitochondrial function is associated with the down-regulation of a large number of metabolic genes. Of these, *Pgc1α* has been identified as the major regulator of mitochondrial biogenesis, and its low expression is highly correlated with obesity and insulin resistance [2,34–36]. Therefore, our aim was to determine whether there was a microRNA that strongly correlates with *Pgc1α* based on the hybridization free energy (hΔG) and could be intimately linked to mitochondrial function and metabolic disorders in skeletal muscle. An in silico analysis was performed through the Sfold2.2 online tool to determine which *Mus musculus* microRNAs bind to *Pgc1α* 3′UTR [37]. From 219 candidates (Supplementary material), *miR-696* had one of the highest hΔG values (−29.8 kcal/mol) in relation to *Pgc1α* 3′UTR (Figure 1). The *miR-696* sequence was paired to extra nucleotide bases in the *Pgc1α* 3′UTR that were not considered by the program as the "seed" region. These observations suggested that *miR-696* has a higher hΔG than the one predicted by the software analysis and may interact with *Pgc1α* mRNA, possibly impairing its expression.

3.2. Pgc1α was targeted by *miR-696*

The gene sequence analysis demonstrated a highly conserved site in the *Pgc1α* mRNA 3′UTR region matching the nucleotide seed sequence of *miR-696*. The conservation of this sequence suggested that *Pgc1α* expression may be regulated by *miR-696* (Figure 2A). To test this hypothesis, we determined the PGC1α protein expression after co-transfection of primary rat myocytes with full-length *Pgc1α* and an oligonucleotide with the same sequence of mature *miR-696* (*miR-696* mimic). The presence of the *miR-696* mimic markedly reduced PGC1α protein expression, indicating that *miR-696* is a strong repressor of *Pgc1α* (Figure 2B). To investigate the physical interactions between *miR-696* and *Pgc1α* 3′UTR, we cloned 245–400 bp of *Pgc1α*-3′UTR mRNA after the GFP sequence and performed a reporter assay overexpressing RFP-miR696 and either GFP-PGC1-3′UTR or a mutant version of the promoter that cannot bind miR696 (GFP-PGC1-3′UTRmt) into HEK 293 cells. Mutation of the PGC1-3′UTR seed region in GFP-PGC1-3′UTRmt plasmid increased the GFP reporter expression, indicating that incomplete binding of miR696 to the 3′UTR region did not block GFP translation (Figure 2C and D). Moreover, given the well-known effect of PGC1α on mitochondrial biogenesis and function [9], we performed an experiment to characterize the impact of *miR-696* on the oxygen consumption rate (OCR) of C2C12 myoblasts. Cells overexpressing *Pgc1α* and transfected with a scrambled sequence of *miR-696* (PGC1α-Scr) increased both the maximal and spare capacity OCR compared to cells co-transfected with an empty vector and a scrambled sequence of *miR-696* (Ev-Scr). PGC1α-Scr showed a tendency of higher basal OCR than cells transfected with both *Pgc1α* and *miR-696* mimic (PGC1α-MiR696), while the maximal and spare capacity significantly increased. Increasing *miR-696* with a *miR-696* mimic (Ev-MiR696) reduced the basal and maximal OCR (Figure 2E and F).

3.3. *miR-696* and Pgc1α had inverse expression profiles

Numerous physiologic conditions are known to regulate *Pgc1α* expression. Basal levels of *Pgc1α* mRNA are higher in slow-twitch oxidative muscles than in more fast-twitch glycolytic muscles [38,39]. Muscle-specific overexpression of *Pgc1α* in mice results in a higher number of slow-twitch fibers in skeletal muscle [39], whereas ablation of *Pgc1α* induces a significant shift from oxidative toward glycolytic muscle fibers [40]. To determine whether skeletal muscle fiber-type composition is associated with *miR-696* and *Pgc1α* expression, we examined gene expression in the soleus, a primarily oxidative muscle, and the extensor digitorum longus (EDL) and tibialis anterior (TA), primarily glycolytic muscles. As expected, *Pgc1α* expression was more abundant in the soleus than in the EDL and TA muscles (Figure 3A). Consistent with our hypothesis, *miR-696* expression was significantly higher in the EDL and TA (Figure 3B), and there was a negative correlation between *Pgc1α* and *miR-696* (Figure 3C).

Another potent regulator of *Pgc1α* expression is metabolic status. We found that *Pgc1α* expression significantly decreased in two animal models of diabetes: STZ-induced diabetic mice and high-fat diet (HFD)-fed mice (Figure 3D and 3E, respectively). These effects were concomitant with an increase in *miR-696* expression (Figure 3D and E). Using C2C12 cells, we found that by day 5 of differentiation, *miR-696* had significantly increased, accompanying a significant decrease in *Pgc1α* compared with their respective controls (Figure 3F). Taken together, these findings demonstrated that there is a negative correlation between *miR-696* and *Pgc1α* expression in mouse skeletal muscle.

3.4. Reduction of *miR-696* protected C2C12 cells from the metabolic effects of palmitic acid overload

Palmitic acid overload is a model commonly used to downregulate mitochondrial function in skeletal muscle cells [30,41]. C2C12 cells exposed to palmitic acid for 24 h exhibited decreased expression of *Pgc1α* and elevated expression of *miR-696* (Figure 4A). We also measured the expression of key mitochondrial genes and found that palmitic acid significantly decreased the expression of cytochrome c (*Cycs*) and the mitochondrial respiratory chain complex IV subunit *Cox5a*. Reduction of *miR-696* using its antisense oligonucleotide (ASO) reversed the effects of palmitic acid, increasing the expression of these two genes, as well as *Pgc1α*, *Tfam*, and *Cs* (Figure 4B). To study mitochondrial function, we evaluated OCR in C2C12 cells and found that palmitic acid reduced both the basal and CCCP-induced OCR, with no effect on the OCR after ATP-synthase inhibition with oligomycin. Transfection of C2C12 cells with *miR-696* ASO before palmitic acid treatment was sufficient to reverse the palmitic acid-induced reduction of OCR (Figure 4C). Increasing *miR-696* with a *miR-696* mimic mirrored the effects of palmitic acid treatment by reducing the basal and oligomycin-induced OCR, tending to decrease the CCCP-induced OCR (Figure 4C).

We next determined whether *miR-696* alters reactive oxygen species (ROS) production in C2C12 cells, since this indicates mitochondrial dysfunction and metabolic stress [30,41]. The addition of palmitic acid increased the rate of H_2O_2 emission in the C2C12 cells, an effect that was reduced by decreasing *miR-696* through transfection of *miR-696* ASO (Figure 4D). There was no effect of *miR-696* mimic on

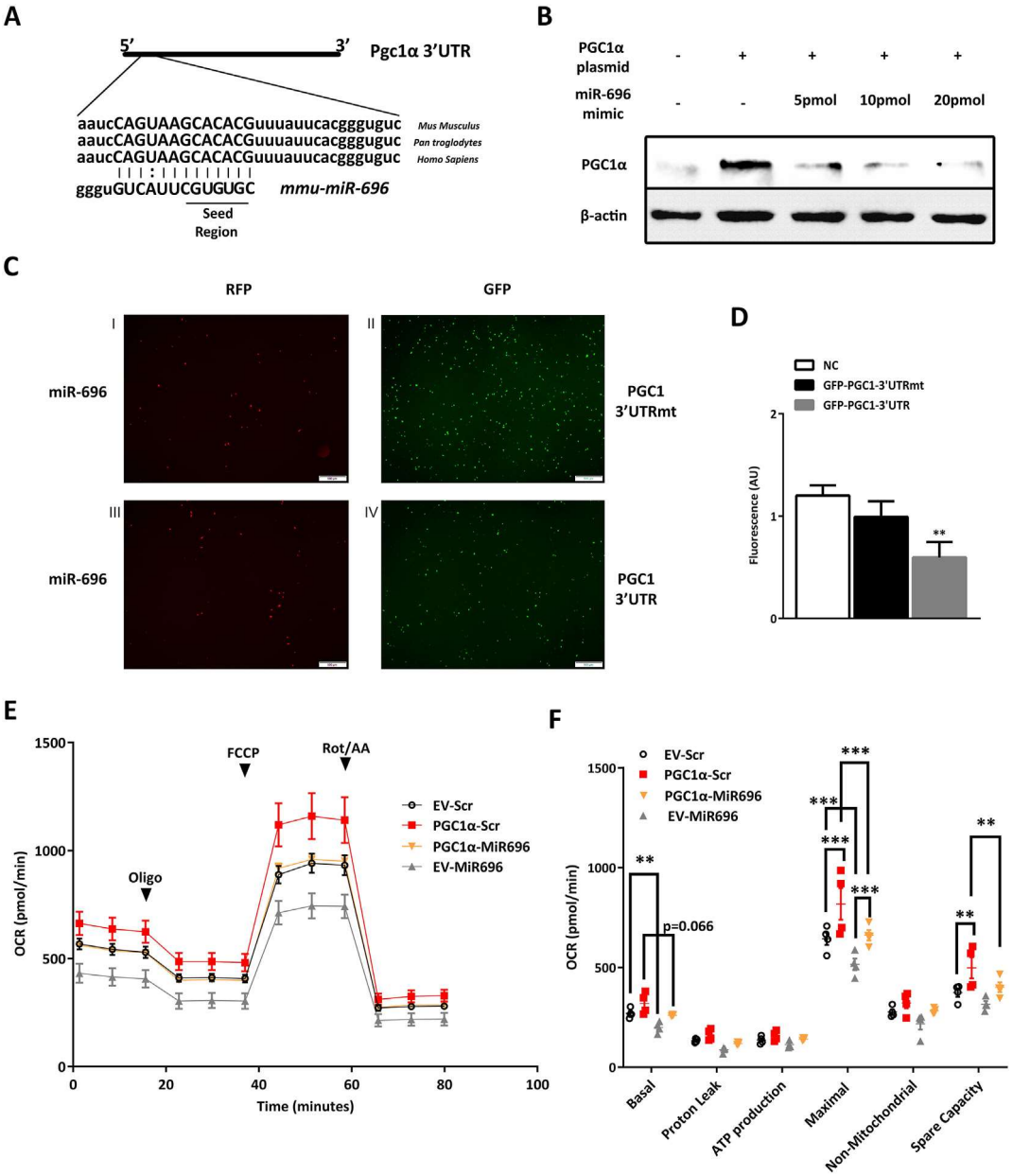

Figure 2: *Pgc1α* was targeted by *miR-696*. (A) The schematic interaction between *miR-696* and *Pgc1α* 3′UTR. (B) Primary rat-cultured cells were transfected with full-length *Pgc1α* plasmid on day 3 of differentiation and then transfected with *miR-696* mimic on day 4 of differentiation. After 24 h, protein was collected and Western blotting was performed to detect *Pgc1α* content (100 μg of protein was loaded). β-actin was used as internal control (n = 2). (C) C2C12 cells were co-transfected either with RFP-*miR-696* and GFP-*Pgc1α*-3′UTR or GFP-*Pgc1α*-3′UTRmt. GFP fluorescence signals were measured to quantify the interactions between *miR-696* and *Pgc1α* 3′UTR (n = 3 experiments). (D) Quantitative analysis of Figure 4C. Scramble oligonucleotide plus GFP (NC) was used as a negative control (white bar), RFP-*miR-696* plus GFP-*Pgc1α*-3′UTRmt (black bar), and RFP-*miR-696* plus GFP-*Pgc1α*-3′UTR (gray bar). (E–F) Cells were transfected with an empty vector and a scrambled oligonucleotide (EV-Scr), *Pgc1α* vector and a scrambled (*Pgc1α*-Scr), *Pgc1α* vector and a *miR-696* mimetic (*Pgc1α*-MiR696), an empty vector, and a *miR-696* mimetic (EV-MiR696) (n = 4). (E) The oxygen consumption rate at a basal state and in the presence of oligomycin, FCCP, and rotenone. (F) Bars indicate the variations in the oxygen consumption rate (ΔOCR, basal = basal − rotenone; uncoupled = oligomycin − rotenone; maximal = FCCP − rotenone) from kinetics depicted in Figure 2E. $^{**}p < 0.01$ and $^{***}p < 0.001$ vs black bar (one-way ANOVA and Tukey's post-test). Each bar indicates mean ± SEM.

H_2O_2 emission in the C2C12 cells relative to the control group (Figure 4D).

Together, these data suggested that metabolic stress can increase *miR-696*, which in turn can downregulate mitochondrial respiration in skeletal muscle cells. Consistent with this finding, we demonstrated that preventing *miR-696* upregulation under metabolically stressful situations can prevent reduction of mitochondrial function in muscle.

3.5. *miR-696* reduced glucose uptake in C2C12 cells

GLUT4 is a major transporter involved in glucose uptake in skeletal muscle cells [42]. Because *Pgc1α* can regulate *Glut4* transcription [43] and glucose uptake [14,44], we investigated whether *miR-696* has an effect on *Glut4* transcription. Plasmid overexpression containing the full-length sequence of *miR-696* (*miR-696*) in C2C12 cells significantly reduced *Pgc1α* and *Glut4* expression (Figure 5A). Consistent with

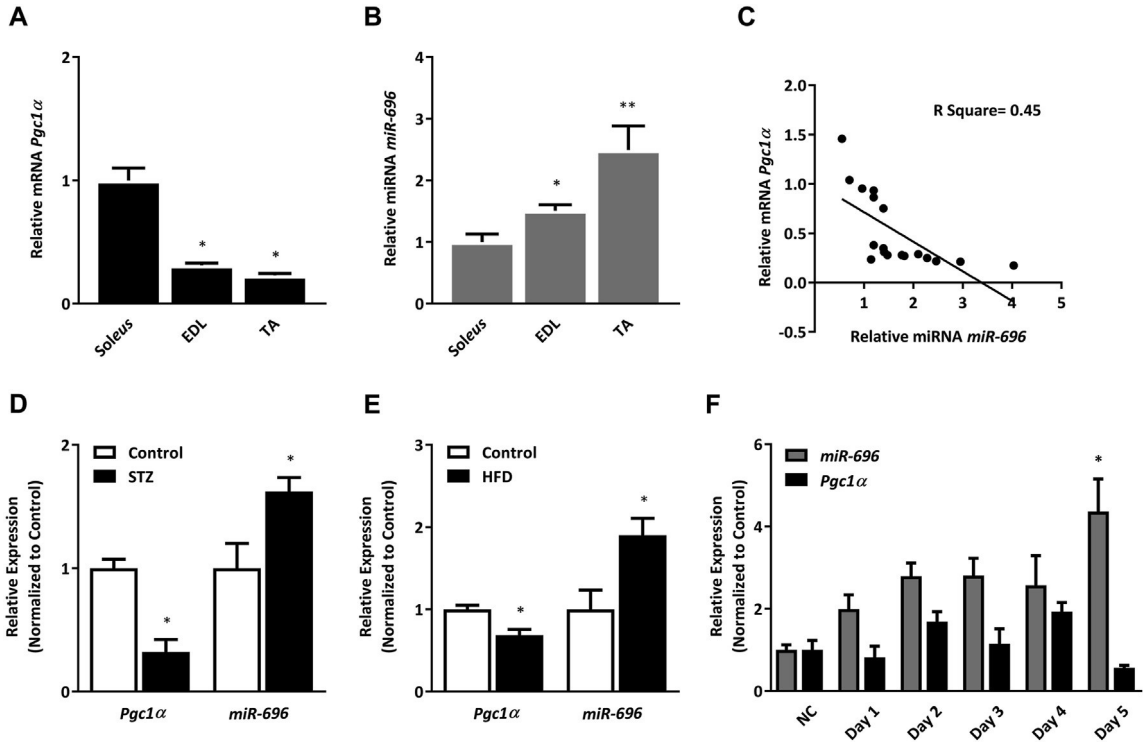

Figure 3: *miR-696 and Pgc1α had inverse expression profiles.* (A) Transcriptional levels of *Pgc1α* expression in the soleus, EDL, and TA muscles from the C57BL/6 mice (n = 6 per group), where comparisons were made between the soleus (oxidative) and EDL and TA (glycolytic) (β-actin was used as a reference gene). (B) Transcriptional levels of *miR-696* expression in the soleus, EDL, and TA muscles from the C57BL/6 mice (n = 6 per group) (*SnoR-202* was used as a reference gene). (C) Correlation between *Pgc1α* and *miR-696* expression through linear regression. (D) Transcriptional levels of *Pgc1α* and *miR-696* in TA muscle from the C57BL/6 mice treated with intravenous injections of streptozotocin (STZ, 70 mg kg^{-1} in overnight fasted mice) or DMSO/saline (control) (n = 5 per group) (β-actin and *SnoR-202* were used as reference genes, respectively). (E) Transcriptional levels of *Pgc1α* and *miR-696* measured in TA muscle from the C57BL/6 mice treated with a normal diet (control) or high-fat diet (HFD) for 10 weeks (n = 5 per group) (β-actin and *SnoR-202* were used as reference genes, respectively). (F) *Pgc1α* and *miR-696* expression measured in C2C12 cells without serum (NC) or with horse serum on days 1, 2, 3, 4, and 5 of differentiation (n = 4) (β-actin and *SnoR-202* were used as reference genes, respectively). **$p < 0.01$ and *$p < 0.05$ (Student's t test, one-way ANOVA, or Tukey's post-test). Each bar indicates mean ± SEM.

decreased Glut4, both basal and insulin-stimulated glucose uptake were significantly reduced in C2C12 cells overexpressing *miR-696* (Figure 5B). We next investigated the effects of *miR-696* on the key insulin signaling intermediary Akt by measuring Akt phosphorylation on the activating site Ser473. Palmitic acid treatment and *miR-696* mimic transfection decreased insulin-stimulated Akt Ser473 phosphorylation. Reducing *miR-696* with *miR-696* ASO partially reversed palmitic acid-induced decreases in Akt phosphorylation (Figure 5C and D). Therefore, our data demonstrated that *miR-696* downregulates glucose uptake and Akt signaling in C2C12 cells.

3.6. Effect of AMPK on *miR-696* expression

AMPK is a key regulator of *Pgc1α* expression and mitochondrial function in skeletal muscle [14,24,45]. In addition, AMPK can regulate GLUT4 transcription and glucose uptake in skeletal muscle, both of which were downregulated by *miR-696* (Figure 5). Therefore, we tested the hypothesis that AMPK may be a negative regulator of *miR-696*. C2C12 cells treated with the AMPK activator AICAR significantly increased *Pgc1α* expression, concomitant with a significant decrease in *miR-696* expression (Figure 6A). We next explored whether mitochondrial function was altered through AICAR treatment in skeletal muscle cells using the oxygen consumption rate (OCR) as our metric. AICAR did not significantly alter basal, oligomycin, or CCCP-stimulated OCR (Figure 6B), but there were significant increases in the concentrations of four tricarboxylic acid (TCA) cycle metabolites (Figure 6C). Because AICAR did not exclusively alter AMPK activity in cells, we determined the specific effects of decreased activity of skeletal muscle AMPKα2, the major isoform expressed in skeletal muscle. Interestingly, AMPKα2 dominant-negative mice (AMPKα2 DN) [46] had reduced *Pgc1α* but no alteration in *miR-696* gene expression (Figure 6D). This suggested that AICAR works through an AMPKα2-independent mechanism to mediate *miR-696* expression and that AMPKα2 may not be a major regulator of *miR-696* in skeletal muscle.

3.7. SNARK regulated *miR-696* expression

Similar to our data demonstrating an increase in *miR-696* by metabolic stress, expression of the AMPK-related kinase *SNARK* was found to be increased in skeletal muscle under several metabolic stress conditions including humans with obesity [47], high-fat diet-fed mice (HFD), and C2C12 cells treated with palmitic acid [29]. Furthermore, SNARK activity is regulated by AICAR [31], thus identifying it as a potential mediator of AICAR-induced *miR-696* expression. Therefore, we hypothesized that *SNARK* may play a regulatory role in *miR-696* expression and consequently *Pgc1α* expression. Genetic knockdown of *Snark* in C2C12 cells by small interfering RNA (siSNARK) significantly reduced *Snark* mRNA (75%) and protein concentrations (60%) (Figure 7A and B, respectively). *Snark* knockdown also resulted in a 38% reduction in *miR-696* expression (Figure 7A) and interestingly resulted in the upregulation of several *Pgc1α*-regulated genes

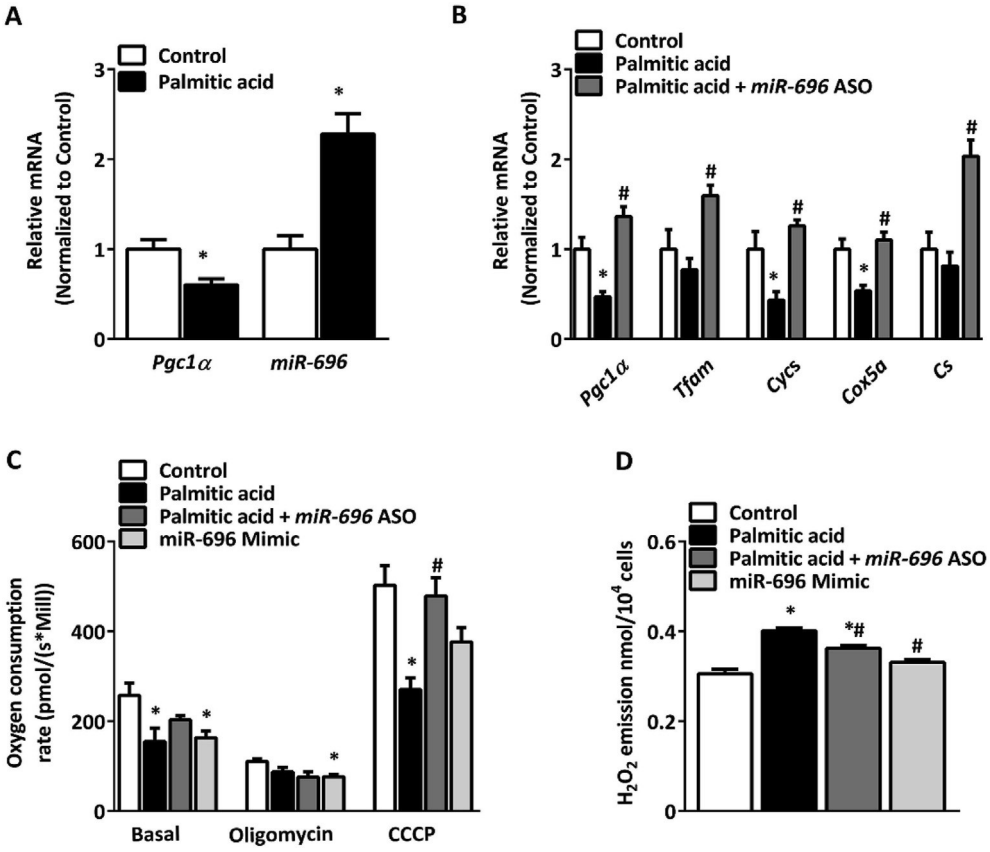

Figure 4: Reduction of miR-696 protected C2C12 cells from the metabolic effects of palmitic acid overload. (A) *Pgc1α* and *miR-696* expression were measured in C2C12 myotubes treated with either ethanol (control) or palmitic acid (700 μM) for 24 h; both groups were treated with vehicle (ethanol in 1% BSA) (n = 3) (β-actin and *SnoR-202* were used as reference genes, respectively). (B) Expression of genes associated with mitochondrial function and biogenesis. Cells were either transfected with scrambled oligonucleotide (control), scrambled oligonucleotide and treated with 700 μM of palmitic acid (palmitic acid), or *miR-696* antisense oligonucleotide and treated with 700 μM of palmitic acid (palmitic acid + *miR-696* ASO). All the groups were treated with vehicle (ethanol in 1% BSA) (n = 5) (β-actin was used as a reference gene). (C and D) Cells were transfected with scrambled oligonucleotide (control), scrambled oligonucleotide and treated with 700 μM of palmitic acid (palmitic acid), *miR-696* antisense oligonucleotide and treated with 700 μM of palmitic acid (palmitic acid + *miR-696* ASO), and *miR-696* full-length oligonucleotide sequence (*miR-696* mimic). All the groups were treated with vehicle (ethanol in 1% BSA) (n = 5). (C) Mitochondrial respiration rate in C2C12 cells. Oligomycin was used as an ATP-synthase inhibitor and CCCP was used for mitochondrial uncoupling (n = 5). (D) Hydrogen peroxide emission as determined by an Amplex UltraRed fluorescent probe after 24 h of palmitic acid treatment (n = 6). *p < 0.05 vs control and #p < 0.05 vs palmitic acid (Student's t test). Each bar indicates mean ± SEM.

(Figure 7C). Consistent with the upregulation of mitochondrial genes, *Snark* knockdown in C2C12 cells resulted in increased basal and maximal OCR, indicating enhanced mitochondrial function (Figure 7D and E). We also found that the overexpression human full-length SNARK in C2C12 cells (Figure 7F) significantly decreased *Pgc1α* expression, while *miR-696* significantly increased (Figure 7G). SNARK overexpression reduced the basal OCR without affecting either the oligomycin or FCCP-induced OCR (Figure 7H and I). These findings suggested that SNARK is a negative regulator of mitochondrial function through the upregulation of *miR-696*.

To investigate SNARK's effects on *miR-696* and *Pgc1α* transcription in vivo, we used a muscle-specific SNARK transgenic mouse line that overexpresses the wild-type human full-length *Snark* sequence (SNARK WT) [29]. TA muscle from SNARK WT had a significant reduction in *Pgc1α* mRNA and a significant increase in *miR-696* compared to control mice (Figure 7J). Thus, in cells and muscles in vivo, alterations in SNARK regulated *miR-696* and *Pgc1α*.

3.8. Modulation of SNARK expression changed spontaneous activity

Functional analysis from metabolic chambers comparing the SNARK WT to the dominant-negative SNARK transgenic mouse (SNARK DN) showed that, regarding overall metabolism, neither the volume of oxygen consumed (VO_2), the respiratory exchange ratio (RER), or the total body energy expenditure (EE) changed between the two strains (Figure 8A—C). However, when we analyzed the total amounts of spontaneous locomotor activity in these mice, we observed a significant reduction in the SNARK WT mouse activity (Figure 8D). Moreover, by performing a maximal endurance capacity test, time spent on the treadmill was lower for the SNARK WT mice (Figure 8E), while the distance tended to be lower (Figure 8F, p = 0.064). No changes in total mice work performed were observed given the reduction of total body weight in the SNARK WT group (Figure 8G). These data revealed the in vivo relevance of the SNARK-*miR696*-*Pgc1α* pathway by demonstrating that the SNARK transgenic mice had altered locomotor activity.

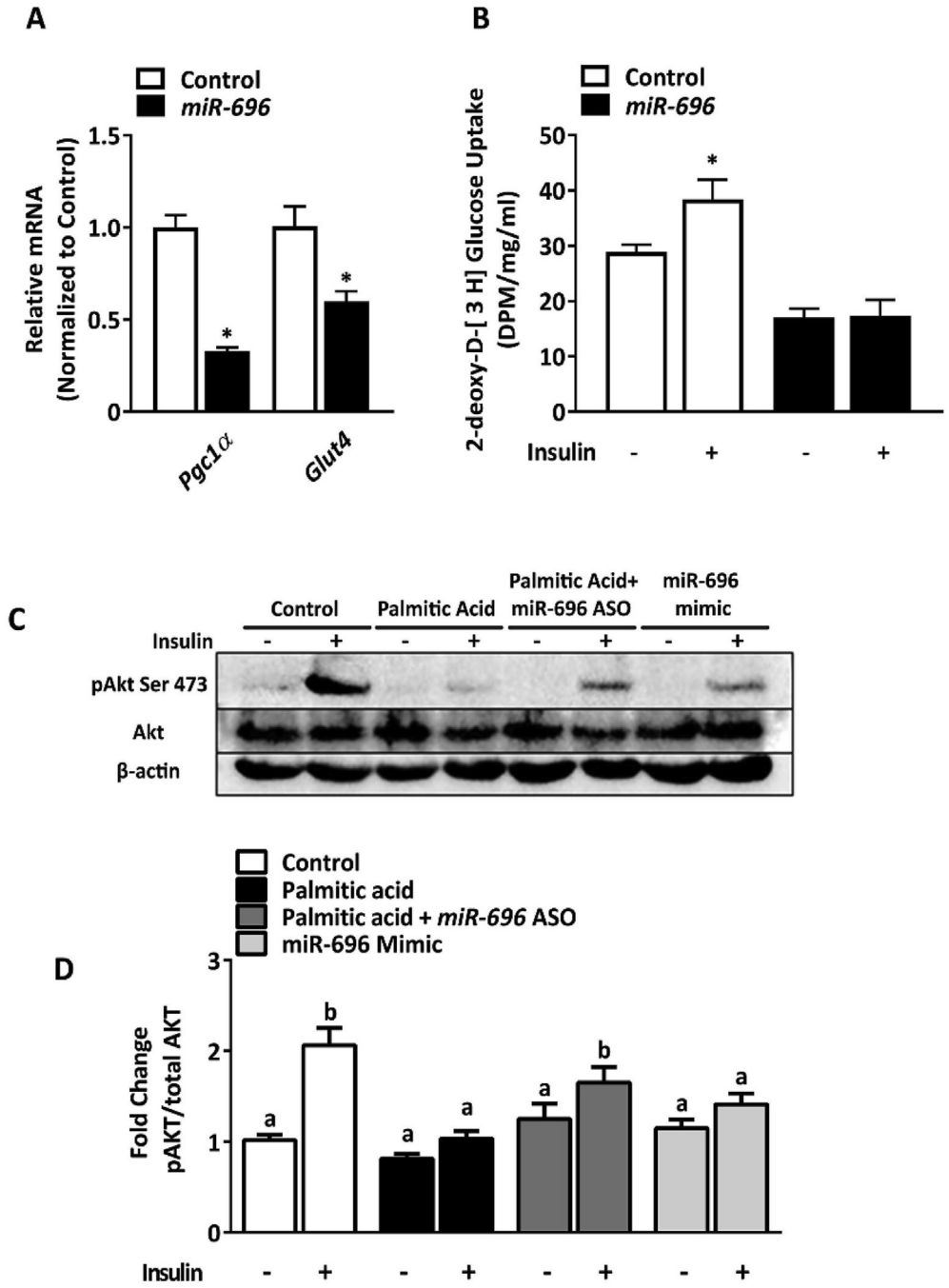

Figure 5: *miR-696 reduced glucose uptake in C2C12 cells.* (A—B) C2C12 cells were transfected with RFP (control) or RFP-*miR-696* (miR-696) (n = 6). (A) Gene expression of *Pgc1α* and *Glut4,* in both the presence and absence of miR-696 (β-actin was used as a reference gene). (B) Glucose uptake was measured with or without insulin (100 nM) in the control and miR-696-transfected groups. (C) C2C12 cells were transfected with scrambled oligonucleotide (control), scrambled oligonucleotide and treated with 700 μM of palmitic acid (palmitic acid), *miR-696* antisense oligonucleotide and treated with 700 μM of palmitic acid (palmitic acid + *miR-696* ASO), and *miR-696* full-length oligonucleotide sequence (*miR-696* mimic). All the groups were treated with vehicle (ethanol in 1% BSA) (n = 5). Western blotting of total Akt (Akt) and phosphorylated Akt on serine 473 (pAkt Ser 473) with or without insulin (100 nM) for 10 min. β-actin (30 μg) was used as an internal control. (D) The bars are a quantification of the Western blotting for the treatment groups represented in panel (C) (n = 3). *p < 0.05 vs control (Student's t test). Each bar indicates mean ± SEM.

4. DISCUSSION

Increased oxidative stress and impaired mitochondrial function are primary contributors to the pathology of type 2 diabetes. Given the large number of people who are affected by metabolic diseases, determining mechanisms that affect mitochondrial function is crucial to developing appropriate prevention and potential therapeutic interventions. Using in silico analysis, we identified *miR-696* as a potentially novel regulator of Pgc1α, a PPARγ co-activator involved in mitochondrial function and biogenesis [48]. Confirming these findings, we observed direct regulation of *Pgc1α* by *miR-696* using a reporter assay (Figure 2C). A similar result was previously validated in primary

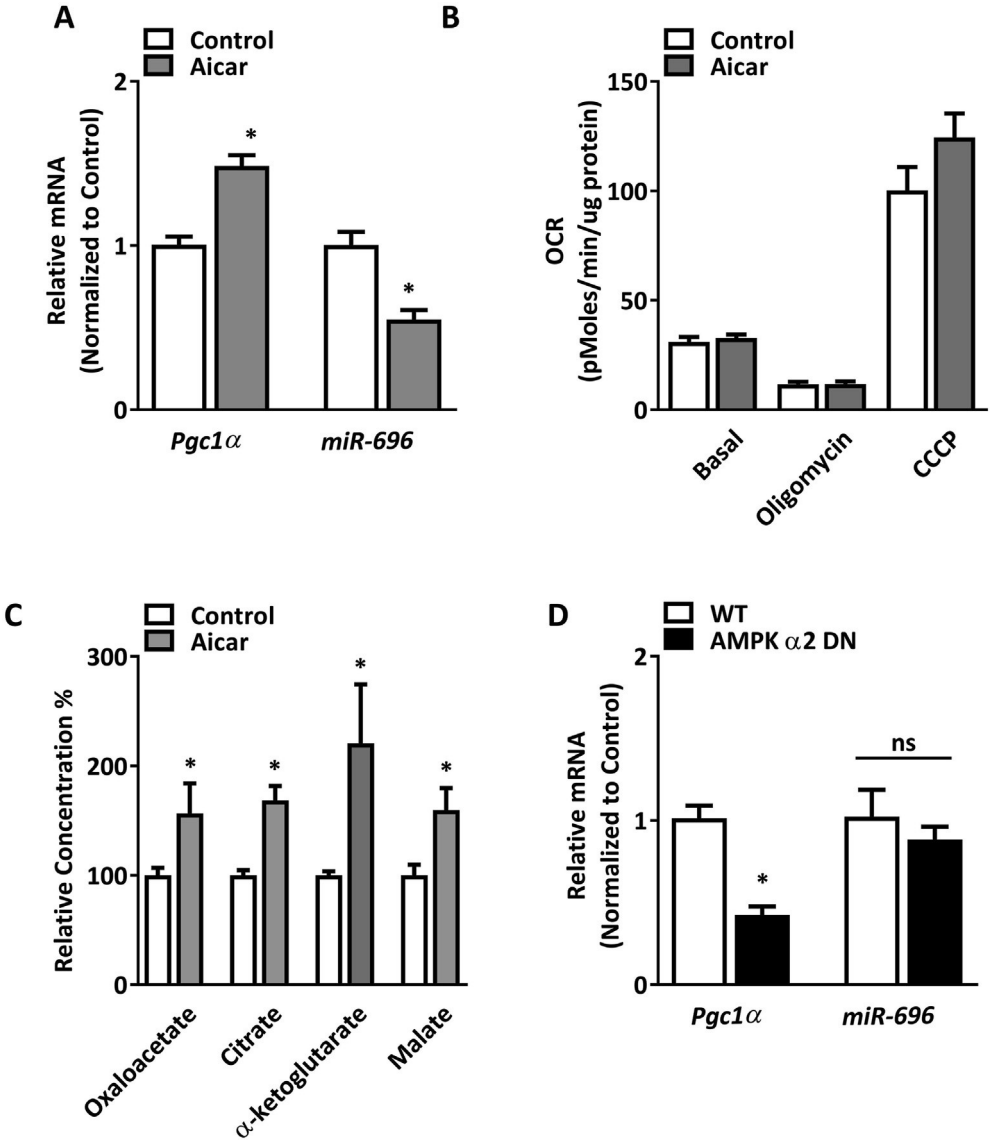

Figure 6: Effect of AMPK on miR-696 expression. (A) *Pgc1α* and *miR-696* expression in C2C12 cells either under control conditions or treated with AICAR (250 μM) (n = 5) (β-actin and *SnoR-202* were used as reference genes, respectively). (B) Mitochondrial respiration rate in C2C12 cells as measured by the oxygen consumption rate (OCR). Oligomycin and CCCP were used for oxidative phosphorylation inhibition and mitochondrial uncoupling, respectively. (C) Tricarboxylic acid (TCA) cycle intermediate concentrations in C2C12 cells treated with AICAR (250 μM) compared to untreated controls (n = 5). (D) *Pgc1α* and *miR-696* expression in the TA muscle from transgenic AMPKα2 DN mice (n = 5). *$p < 0.05$ vs control (Student's t test). Each bar indicates mean ± SEM.

hepatocytes through an experiment using a luciferase reporter assay [49]. In addition, *Pgc1α* content was markedly reduced in skeletal muscle cells exposed to increasing concentrations of *miR-696* mimic (Figure 2B). Thus, our data established *miR-696* as a novel suppressor of Pgc1α expression.

As Pgc1α is a critical regulator of mitochondrial function, we next sought to determine the physiological implications of changes in *miR-696* expression in skeletal muscle using in vitro and in vivo models. *Pgc1α* expression has been shown to be higher in skeletal muscles predominantly composed of oxidative (type I) fibers compared to skeletal muscle tissues mainly composed of glycolytic (type II) fibers [50—52]. In the current study, we found a negative correlation between *miR-696* and *Pgc1α* expression in muscle, with oxidative muscle having lower *miR-696* and higher Pgc1a levels than glycolytic muscle. Thus, our data identified *miR-696* as a potential mechanism for differential *Pgc1α* expression and mitochondrial content in skeletal muscles with different metabolic characteristics (Figure 3C).

Our data demonstrated that the expression of *miR-696* increased in the skeletal muscle of C57BL/6 mice exposed to streptozotocin or a high-fat diet (Figure 3D and E), both of which are well-known models for inducing metabolic stress and reducing mitochondrial function [34,45,53]. We also observed increased expression of *mir-696* throughout the differentiation process of C2C12 cells (Figure 3F). Interestingly, inhibition of *miR-696* was shown to accelerate differentiation in 3D-engineered human skeletal muscle bundles [54]. In addition, we showed that C2C12 cells exposed to a high dose of palmitic acid had elevated *miR-696*, and the transfection of C2C12 cells with a *miR-696* oligonucleotide mimic reduced both *Pgc1α* expression and basal oxygen consumption. These effects were associated with increased reactive oxygen species production and low

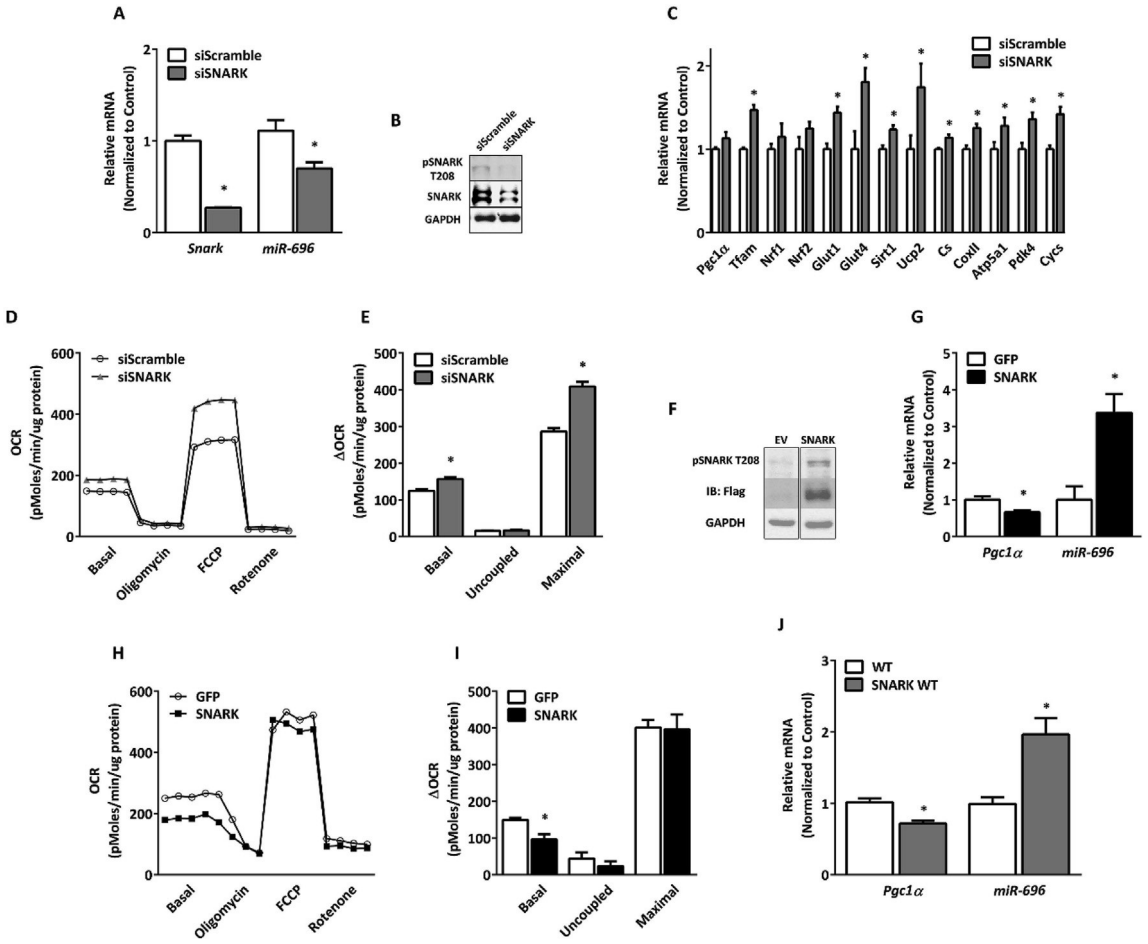

Figure 7: SNARK regulated *miR-696* expression. (A—E) C2C12 cells were transfected with scrambled oligonucleotide (control) or siSNARK oligonucleotide (siSNARK) for 48 h (n = 3). (A) Comparison of Snark and *miR-696* gene expression with and without oligonucleotide transfection (Gapdh and *SnoR-202* were used as reference genes, respectively). (B) Total and phosphorylated SNARK protein content. GAPDH was used as a loading control; 30 μg of protein was loaded. (C) Gene expression analysis of mitochondrial-related genes in skeletal muscle: *Pgc1α*, *Tfam*, *Nrf1*, *Nrf2*, *Sirt1*, *Ucp2*, *Cs CoxII*, *Atp5a1*, *Pdk4*, and *Cycs* and glucose metabolism-related genes *Glut1* and *Glut4* in skeletal muscle. (D) The oxygen consumption rate at a basal state and in the presence of oligomycin, FCCP, and rotenone. (E) Bars indicate the variations in the oxygen consumption rate (ΔOCR, basal = basal − rotenone; uncoupled = oligomycin − rotenone; maximal = FCCP − rotenone) from kinetics depicted in (D). (F—I) C2C12 cells were transfected with GFP or empty vector (EV) or SNARK vector (SNARK) for 48 h (n = 3). (F) Protein expression of Flag and phosphorylated SNARK protein content. GAPDH (30 μg) was used as a loading control. (G) *Pgc1α* and *miR-696* gene expression (Gapdh and *SnoR-202* were used as reference genes, respectively). (H) Oxygen consumption rate at a basal state and in the presence of oligomycin, FCCP, and rotenone. (I) Bars indicate the difference in the oxygen consumption rate between the treatment and control groups under different metabolic conditions (basal = basal − rotenone; uncoupled = oligomycin − rotenone; maximal = FCCP − rotenone). Bar graph of the kinetics depicted in Figure 7H. (J) *Pgc1α* and *miR-696* gene expression in TA muscle from overexpressing SNARK wild-type (SNARK WT) compared to wild-type control mice (WT) (n = 5) (Gapdh and *SnoR-202* were used as reference genes, respectively). *p < 0.05 (Student's t test). Each bar indicates mean ± SEM.

levels of several mitochondrial biogenesis-related genes, indicating a close relationship between *miR-696* expression and mitochondrial function. In contrast, *miR-696* knockdown partially reversed the effects of fatty acid overload on mitochondrial function in muscle cells (Figure 4). Thus, our data identified *miR-696* as a novel regulator of mitochondrial function in response to metabolic stress in muscle.

AMPK, an intracellular energetic sensor, has been described as a positive mediator of *Pgc1α* expression by direct phosphorylation of the Pgc1a promoter in myotubes [14]. Herein, we demonstrated that AICAR, a well-known activator of AMPK, can upregulate *Pgc1α* and downregulate *miR-696* expression, suggesting AMPK as a potential mediator of our newly discovered *miR-696*/Pgc1α axis. However, we observed no effect of AMPK on *miR-696* expression in skeletal muscle of mice overexpressing AMPK with a dominant-negative mutation at the α2 subunit (Figure 6D), suggesting that a target other than AMPK may be responsible for AICAR-induced regulation of *miR-696*/Pgc1α.

The AMPK-related kinase SNARK has been associated with multiple cellular processes including glucose transport during skeletal muscle contraction [55], metabolic stress [47], and regulation of skeletal muscle mass and cell survival [29]. Interestingly, a gradual increase in SNARK expression during differentiation of C2C12 cells and a gradual reduction of *Pgc1α* expression in C2C12 cells throughout differentiation [56] were demonstrated. Furthermore, SNARK expression was markedly increased in human cultured myocytes in response to metabolic stressors including palmitate and TNFα, two conditions well known to decrease PGC1α transcription [47]. Given previous evidence that SNARK and Pgc1α are divergently regulated, we hypothesized that SNARK may be a negative regulator of Pgc1a expression via *miR-696*. In line with this hypothesis, we found that overexpression of SNARK caused a reduction in the *Pgc1α* expression and mitochondrial oxygen consumption rate in C2C12 cells (Figure 7G and H). Importantly, the impact of SNARK overexpression on Pgc1a

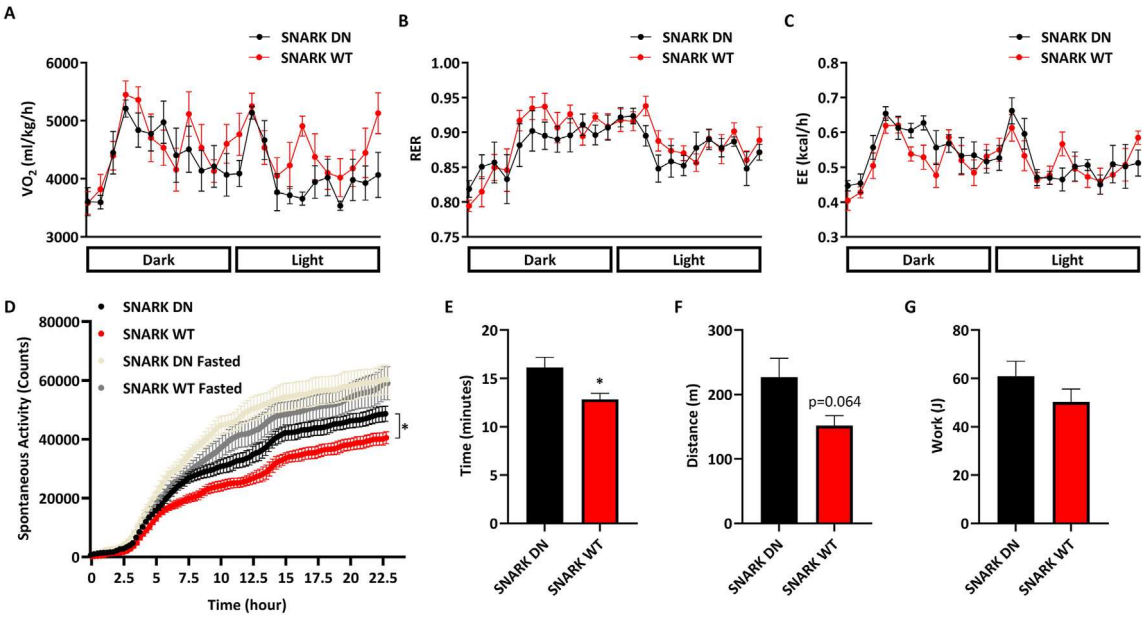

Figure 8: Modulation of SNARK expression changed spontaneous activity. (A–C) ANCOVA analysis of SNARK DN and SNARK WT mice housed under 22 °C in metabolic cages. (A) Volume of oxygen (VO_2) consumed over time. (B) Respiratory exchange ratio (RER) over time. (C) Energy expenditure (EE) over time. (D) ANCOVA analysis of cumulative activity over time of fed and fasted SNARK DN and SNARK WT mice housed under 22 °C in metabolic cages. (E) Time, (F) distance, (G) and work achieved by SNARK DN and SNARK WT mice on a maximal endurance performance test (running on a treadmill until exhaustion). *$p < 0.05$ (Student's t test or 2-way ANOVA). Graphs are mean ± SEM.

expression and mitochondrial function occurred in conjunction with increased *miR-696* transcription in C2C12 cells and SNARK transgenic mice (Figure 7G and J). Thus, our data identified a novel role of SNARK in regulating mitochondrial function through the *miR-696*/Pgc1a axis.

The physiological purpose of this newly discovered SNARK-*miR-696*-*Pgc1α* axis is not known. However, we have previously shown that SNARK is necessary to prevent apoptosis in muscle cells exposed to metabolic stressors such as palmitate [29]. Moreover, we have demonstrated that loss of SNARK activity leads to accelerated loss of muscle mass with age. Thus, previous evidence indicated that SNARK plays a protective role in muscle by preventing apoptosis and muscle loss under metabolic and physiological stress conditions. We postulate that the protective effect of SNARK on myocyte survival may be due in part to its ability to reduce Pgc1α expression via *miR-696*. In line with that assertion, mice overexpressing *Pgc1α* exhibited severe muscle atrophy, leading to a 25% reduction in body weight by 25 weeks of age [57]. In addition, mice overexpressing *Pgc1α* in muscle were more prone to fat-induced insulin resistance and had no metabolic improvements in response to exercise or caloric restriction [58,59]. These data indicated that an overabundance of mitochondrial activity had a deleterious effect on cellular function and myocyte survival. In support of this, long-term overexpression of *PGC1β*, a member of the PGC family, induced mitochondrial biogenesis and activity and apoptosis [60]. Thus, although increased mitochondrial function is often thought to be a positive adaptation, SNARK may play an important role in limiting excess mitochondrial activity during times of metabolic increases, protecting cells from mitochondria-induced apoptosis.

It is important to acknowledge that *miR-696* is a mouse-specific microRNA and was studied in the context of metabolic stress. We believe that it is crucial to search for microRNAs that can regulate mitochondrial biogenesis through PGC1A in human cells and provide biological relevance for humans. For this reason, we performed an "in silico" analysis (TargetScanHuman prediction toll) using the human 3′UTR of the PGC1A gene and found the human microRNA hsa-miR-218-5p sitting exactly on the same region targeted by the microRNA miR-696 in the mouse 3′UTR of the Pgc1α gene. Interestingly, hsa-mir-218 was found to be increased in urinary exosomes of type 1 diabetic children [61]. In another study, hsa-mir-218-5p was reduced in gastric cancer cells allowing metastatic behavior, which could be associated with an increase in PGC1A expression [62]. Moreover, "in silico" analysis four microRNAs mitochondrial sub-localization indicated that hsa-mir-218-5p is located in the mitochondria [63]. Taken together, this suggests that microRNA hsa-mir-218-5p may regulate PGC1A in humans and indicates a possible regulatory function of hsa-mir-218-5p over mitochondrial homeostasis.

5. CONCLUSION

In conclusion, we provided evidence of a mechanism in which high levels of metabolic stress in skeletal muscle cells increased the microRNA *miR-696* levels and reduced Pgc1α expression and mitochondrial function. We also identified SNARK as a novel regulator of mitochondrial function via *miR-696* and Pgc1α. These findings could lead to novel therapeutic and preventive strategies for metabolic diseases, including type 2 diabetes.

ACKNOWLEDGMENTS

This study was supported by the State Science-Funding Agency FAPESP (2013/22733-0), National Institutes of Health grants R01DK099511 (to L.J.G.), and the Joslin Diabetes Center DRC (P30 DK36836). CAPES sponsored the first author via a doctorate scholarship 99999.009038/2014-00. Special thanks to Alison Slack for proofreading this work.

CONFLICT OF INTEREST

None declared.

APPENDIX A. SUPPLEMENTARY DATA

Supplementary data to this article can be found online at https://doi.org/10.1016/j.molmet.2021.101226.

REFERENCES

[1] Perry, R.J., Zhang, D., Zhang, X.-M., Boyer, J.L., Shulman, G.I., 2015. Controlled-release mitochondrial protonophore reverses diabetes and steatohepatitis in rats. Science 347:1253—1256.

[2] Mootha, V.K., Lindgren, C.M., Eriksson, K.-F., Subramanian, A., Sihag, S., Lehar, J., et al., 2003. PGC-1alpha-responsive genes involved in oxidative phosphorylation are coordinately downregulated in human diabetes. Nature Genetics 34:267—273.

[3] Pal, M., Wunderlich, C.M., Spohn, G., Brönneke, H.S., Schmidt-Supprian, M., Wunderlich, F.T., 2013. Alteration of JNK-1 signaling in skeletal muscle fails to affect glucose homeostasis and obesity-associated insulin resistance in mice. PLoS One 8:e54247.

[4] Kodama, K., Toda, K., Morinaga, S., Yamada, S., Butte, A.J., 2015. Anti-CD44 antibody treatment lowers hyperglycemia and improves insulin resistance, adipose inflammation, and hepatic steatosis in diet-induced obese mice. Diabetes 64:867—875.

[5] Wueest, S., Rapold, R.A., Schumann, D.M., Rytka, J.M., Schildknecht, A., Nov, O., et al., 2010. Deletion of Fas in adipocytes relieves adipose tissue inflammation and hepatic manifestations of obesity in mice. Journal of Clinical Investigation 120:191—202.

[6] Wright, D.C., Han, D.-H., Garcia-Roves, P.M., Geiger, P.C., Jones, T.E., Holloszy, J.O., 2007. Exercise-induced mitochondrial biogenesis begins before the increase in muscle PGC-1alpha expression. Journal of Biological Chemistry 282:194—199.

[7] Bocco, B.M.L.C., Louzada, R.A.N., Silvestre, D.H.S., Santos, M.C.S., Anne-Palmer, E., Rangel, I.F., et al., 2016. Thyroid hormone activation by type 2 deiodinase mediates exercise-induced peroxisome proliferator-activated receptor-γ coactivator-1α expression in skeletal muscle. Journal of Physiology (London) 594:5255—5269.

[8] Cho, Y., Hazen, B.C., Russell, A.P., Kralli, A., 2013. Peroxisome proliferator-activated receptor γ coactivator 1 (PGC-1)- and estrogen-related receptor (ERR)-induced regulator in muscle 1 (Perm1) is a tissue-specific regulator of oxidative capacity in skeletal muscle cells. Journal of Biological Chemistry 288:25207—25218.

[9] Lin, J., Handschin, C., Spiegelman, B.M., 2005. Metabolic control through the PGC-1 family of transcription coactivators. Cell Metabolism 1:361—370.

[10] Arany, Z., 2008. PGC-1 coactivators and skeletal muscle adaptations in health and disease. Current Opinion in Genetics & Development 18:426—434.

[11] Safdar, A., Little, J.P., Stokl, A.J., Hettinga, B.P., Akhtar, M., Tarnopolsky, M.A., 2011. Exercise increases mitochondrial PGC-1alpha content and promotes nuclear-mitochondrial cross-talk to coordinate mitochondrial biogenesis. Journal of Biological Chemistry 286:10605—10617.

[12] Scarpulla, R.C., 2006. Nuclear control of respiratory gene expression in mammalian cells. Journal of Cellular Biochemistry 97:673—683.

[13] Ruas, J.L., White, J.P., Rao, R.R., Kleiner, S., Brannan, K.T., Harrison, B.C., et al., 2012. A PGC-1α isoform induced by resistance training regulates skeletal muscle hypertrophy. Cell 151:1319—1331.

[14] Jäger, S., Handschin, C., St-Pierre, J., Spiegelman, B.M., 2007. AMP-activated protein kinase (AMPK) action in skeletal muscle via direct phosphorylation of PGC-1alpha. Proceedings of the National Academy of Sciences of the United States of America 104:12017—12022.

[15] Nemoto, S., Fergusson, M.M., Finkel, T., 2005. SIRT1 functionally interacts with the metabolic regulator and transcriptional coactivator PGC-1{alpha}. Journal of Biological Chemistry 280:16456—16460.

[16] Bartel, D.P., 2009. MicroRNAs: target recognition and regulatory functions. Cell 136:215—233.

[17] Sun, L.-Y., Wang, N., Ban, T., Sun, Y.-H., Han, Y., Sun, L.-L., et al., 2014. MicroRNA-23a mediates mitochondrial compromise in estrogen deficiency-induced concentric remodeling via targeting PGC-1α. Journal of Molecular and Cellular Cardiology 75:1—11.

[18] Xu, Y., Zhao, C., Sun, X., Liu, Z., Zhang, J., 2015. MicroRNA-761 regulates mitochondrial biogenesis in mouse skeletal muscle in response to exercise. Biochemical and Biophysical Research Communications 467:103—108.

[19] Mineno, J., Okamoto, S., Ando, T., Sato, M., Chono, H., Izu, H., et al., 2006. The expression profile of microRNAs in mouse embryos. Nucleic Acids Research 34:1765—1771.

[20] Aoi, W., Naito, Y., Mizushima, K., Takanami, Y., Kawai, Y., Ichikawa, H., et al., 2010. The microRNA miR-696 regulates PGC-1{alpha} in mouse skeletal muscle in response to physical activity. American Journal of Physiology. Endocrinology and Metabolism 298:E799—E806.

[21] Wen, F., Zhang, H., Bao, C., Yang, M., Wang, N., Zhang, J., et al., 2015. Resistin increases ectopic deposition of lipids through miR-696 in C2C12 cells. Biochemical Genetics 53:63—71.

[22] Xiao, B., Sanders, M.J., Underwood, E., Heath, R., Mayer, F.V., Carmena, D., et al., 2011. Structure of mammalian AMPK and its regulation by ADP. Nature 472:230—233.

[23] Teodoro, B.G., Sampaio, I.H., Bomfim, L.H.M., Queiroz, A.L., Silveira, L.R., Souza, A.O., et al., 2017. Long-chain acyl-CoA synthetase 6 regulates lipid synthesis and mitochondrial oxidative capacity in human and rat skeletal muscle. The Journal of Physiology 595:677—693.

[24] Palacios, O.M., Carmona, J.J., Michan, S., Chen, K.Y., Manabe, Y., Ward, J.L., et al., 2009. Diet and exercise signals regulate SIRT3 and activate AMPK and PGC-1alpha in skeletal muscle. Aging 1:771—783.

[25] Koh, H.-J., Arnolds, D.E., Fujii, N., Tran, T.T., Rogers, M.J., Jessen, N., et al., 2006. Skeletal muscle-selective knockout of LKB1 increases insulin sensitivity, improves glucose homeostasis, and decreases TRB3. Molecular and Cellular Biology 26:8217—8227.

[26] Thirugnanam, K., Cossette, S.M., Lu, Q., Chowdhury, S.R., Harmann, L.M., Gupta, A., et al., 2019. Cardiomyocyte-specific Snrk prevents inflammation in the heart. Journal of the American Heart Association 8:e012792.

[27] Rines, A.K., Chang, H.-C., Wu, R., Sato, T., Khechaduri, A., Kouzu, H., et al., 2017. Snf1-related kinase improves cardiac mitochondrial efficiency and decreases mitochondrial uncoupling. Nature Communications 8:14095.

[28] Li, J., An, R., Lai, S., Li, L., Liu, S., Xu, H., 2019. Dysregulation of PP2A-Akt interaction contributes to sucrose non-fermenting related kinase (SNRK) deficiency induced insulin resistance in adipose tissue. Molecular Metabolism 28:26—35.

[29] Lessard, S.J., Rivas, D.A., So, K., Koh, H.-J., Queiroz, A.L., Hirshman, M.F., et al., 2016. The AMPK-related kinase SNARK regulates muscle mass and myocyte survival. Journal of Clinical Investigation 126:560—570.

[30] Barbosa, M.R., Sampaio, I.H., Teodoro, B.G., Sousa, T.A., Zoppi, C.C., Queiroz, A.L., et al., 2013. Hydrogen peroxide production regulates the mitochondrial function in insulin resistant muscle cells: effect of catalase overexpression. Biochimica et Biophysica Acta 1832:1591—1604.

[31] Kuga, W., Tsuchihara, K., Ogura, T., Kanehara, S., Saito, M., Suzuki, A., et al., 2008. Nuclear localization of SNARK; its impact on gene expression. Biochemical and Biophysical Research Communications 377:1062—1066.

[32] Fujii, N., Hirshman, M.F., Kane, E.M., Ho, R.C., Peter, L.E., Seifert, M.M., et al., 2005. AMP-activated protein kinase alpha2 activity is not essential for contraction- and hyperosmolarity-induced glucose transport in skeletal muscle. Journal of Biological Chemistry 280:39033—39041.

[33] Barré, L., Richardson, C., Hirshman, M.F., Brozinick, J., Fiering, S., Kemp, B.E., et al., 2007. Genetic model for the chronic activation of skeletal

muscle AMP-activated protein kinase leads to glycogen accumulation. American Journal of Physiology. Endocrinology and Metabolism 292:E802—E811.

[34] Patti, M.E., Butte, A.J., Crunkhorn, S., Cusi, K., Berria, R., Kashyap, S., et al., 2003. Coordinated reduction of genes of oxidative metabolism in humans with insulin resistance and diabetes: potential role of PGC1 and NRF1. Proceedings of the National Academy of Sciences of the United States of America 100:8466—8471.

[35] Zhang, Y., Yang, L., Gao, Y.-F., Fan, Z.-M., Cai, X.-Y., Liu, M.-Y., et al., 2013. MicroRNA-106b induces mitochondrial dysfunction and insulin resistance in C2C12 myotubes by targeting mitofusin-2. Molecular and Cellular Endocrinology 381:230—240.

[36] Greene, N.P., Lee, D.E., Brown, J.L., Rosa, M.E., Brown, L.A., Perry, R.A., et al., 2015. Mitochondrial quality control, promoted by PGC-1α, is dysregulated by Western diet-induced obesity and partially restored by moderate physical activity in mice. Physiological Reports 3.

[37] Ding, Y., Lawrence, C.E., 2001. Statistical prediction of single-stranded regions in RNA secondary structure and application to predicting effective antisense target sites and beyond. Nucleic Acids Research 29:1034—1046.

[38] Wang, L., Jia, Y., Rogers, H., Suzuki, N., Gassmann, M., Wang, Q., et al., 2013. Erythropoietin contributes to slow oxidative muscle fiber specification via PGC-1α and AMPK activation. The International Journal of Biochemistry & Cell Biology 45:1155—1164.

[39] Lin, J., Wu, H., Tarr, P.T., Zhang, C.-Y., Wu, Z., Boss, O., et al., 2002. Transcriptional co-activator PGC-1 alpha drives the formation of slow-twitch muscle fibres. Nature 418:797—801.

[40] Zechner, C., Lai, L., Zechner, J.F., Geng, T., Yan, Z., Rumsey, J.W., et al., 2010. Total skeletal muscle PGC-1 deficiency uncouples mitochondrial derangements from fiber type determination and insulin sensitivity. Cell Metabolism 12:633—642.

[41] Anderson, E.J., Lustig, M.E., Boyle, K.E., Woodlief, T.L., Kane, D.A., Lin, C.-T., et al., 2009. Mitochondrial H_2O_2 emission and cellular redox state link excess fat intake to insulin resistance in both rodents and humans. Journal of Clinical Investigation 119:573—581.

[42] Tsuchiya, A., Kanno, T., Nishizaki, T., 2014. PI3 kinase directly phosphorylates Akt1/2 at Ser473/474 in the insulin signal transduction pathway. Journal of Endocrinology 220:49—59.

[43] Michael, L.F., Wu, Z., Cheatham, R.B., Puigserver, P., Adelmant, G., Lehman, J.J., et al., 2001. Restoration of insulin-sensitive glucose transporter (GLUT4) gene expression in muscle cells by the transcriptional coactivator PGC-1. Proceedings of the National Academy of Sciences of the United States of America 98:3820—3825.

[44] McGee, S.L., van Denderen, B.J.W., Howlett, K.F., Mollica, J., Schertzer, J.D., Kemp, B.E., et al., 2008. AMP-activated protein kinase regulates GLUT4 transcription by phosphorylating histone deacetylase 5. Diabetes 57:860—867.

[45] Franko, A., von Kleist-Retzow, J.C., Böse, M., Sanchez-Lasheras, C., Brodesser, S., Krut, O., et al., 2012. Complete failure of insulin-transmitted signaling, but not obesity-induced insulin resistance, impairs respiratory chain function in muscle. Journal of Molecular Medicine 90:1145—1160.

[46] Musi, N., Hirshman, M.F., Arad, M., Xing, Y., Fujii, N., Pomerleau, J., et al., 2005. Functional role of AMP-activated protein kinase in the heart during exercise. FEBS Letters 579:2045—2050.

[47] Rune, A., Osler, M.E., Fritz, T., Zierath, J.R., 2009. Regulation of skeletal muscle sucrose, non-fermenting 1/AMP-activated protein kinase-related kinase (SNARK) by metabolic stress and diabetes. Diabetologia 52:2182—2189.

[48] Rohas, L.M., St-Pierre, J., Uldry, M., Jäger, S., Handschin, C., Spiegelman, B.M., 2007. A fundamental system of cellular energy homeostasis regulated by PGC-1alpha. Proceedings of the National Academy of Sciences of the United States of America 104:7933—7938.

[49] Fang, Z., Li, P., Jia, W., Jiang, T., Wang, Z., Xiang, Y., 2016. miR-696 plays a role in hepatic gluconeogenesis in ob/ob mice by targeting PGC-1α. International Journal of Molecular Medicine 38:845—852.

[50] Rasbach, K.A., Gupta, R.K., Ruas, J.L., Wu, J., Naseri, E., Estall, J.L., et al., 2010. PGC-1alpha regulates a HIF2alpha-dependent switch in skeletal muscle fiber types. Proceedings of the National Academy of Sciences of the United States of America 107:21866—21871.

[51] Handschin, C., Chin, S., Li, P., Liu, F., Maratos-Flier, E., Lebrasseur, N.K., et al., 2007. Skeletal muscle fiber-type switching, exercise intolerance, and myopathy in PGC-1alpha muscle-specific knock-out animals. Journal of Biological Chemistry 282:30014—30021.

[52] Matsuura, T., Li, Y., Giacobino, J.-P., Fu, F.H., Huard, J., 2007. Skeletal muscle fiber type conversion during the repair of mouse soleus: potential implications for muscle healing after injury. Journal of Orthopaedic Research 25:1534—1540.

[53] Rocha-Rodrigues, S., Rodríguez, A., Gouveia, A.M., Gonçalves, I.O., Becerril, S., Ramírez, B., et al., 2016. Effects of physical exercise on myokines expression and brown adipose-like phenotype modulation in rats fed a high-fat diet. Life Sciences 165:100—108.

[54] Cheng, C.S., Ran, L., Bursac, N., Kraus, W.E., Truskey, G.A., 2016. Cell density and Joint microRNA-133a and microRNA-696 inhibition enhance differentiation and contractile function of engineered human skeletal muscle tissues. Tissue Engineering Part A 22:573—583.

[55] Koh, H.-J., Toyoda, T., Fujii, N., Jung, M.M., Rathod, A., Middelbeek, R.J.-W., et al., 2010. Sucrose nonfermenting AMPK-related kinase (SNARK) mediates contraction-stimulated glucose transport in mouse skeletal muscle. Proceedings of the National Academy of Sciences of the United States of America 107:15541—15546.

[56] Adamovich, Y., Shlomai, A., Tsvetkov, P., Umansky, K.B., Reuven, N., Estall, J.L., et al., 2013. The protein level of PGC-1α, a key metabolic regulator, is controlled by NADH-NQO1. Molecular and Cellular Biology 33:2603—2613.

[57] Miura, S., Tomitsuka, E., Kamei, Y., Yamazaki, T., Kai, Y., Tamura, M., et al., 2006. Overexpression of peroxisome proliferator-activated receptor gamma co-activator-1alpha leads to muscle atrophy with depletion of ATP. American Journal Of Pathology 169:1129—1139.

[58] Choi, C.S., Befroy, D.E., Codella, R., Kim, S., Reznick, R.M., Hwang, Y.-J., et al., 2008. Paradoxical effects of increased expression of PGC-1alpha on muscle mitochondrial function and insulin-stimulated muscle glucose metabolism. Proceedings of the National Academy of Sciences of the United States of America 105:19926—19931.

[59] Wong, K.E., Mikus, C.R., Slentz, D.H., Seiler, S.E., DeBalsi, K.L., Ilkayeva, O.R., et al., 2015. Muscle-specific overexpression of PGC-1α does not augment metabolic improvements in response to exercise and caloric restriction. Diabetes 64:1532—1543.

[60] Sopariwala, D.H., Yadav, V., Badin, P.-M., Likhite, N., Sheth, M., Lorca, S., et al., 2017. Long-term PGC1β overexpression leads to apoptosis, autophagy and muscle wasting. Scientific Reports 7:10237.

[61] Kong, Q., Guo, X., Guo, Z., Su, T., 2019. Urinary exosome miR-424 and miR-218 as biomarkers for type 1 diabetes in children. Clinical Laboratory 65.

[62] Lin, J., Zhang, Y., Zeng, X., Xue, C., Lin, X., 2020. Circrna circrims acts as a microrna sponge to promote gastric cancer metastasis. ACS Omega 5: 23237—23246.

[63] Yan, L.-R., Wang, A., Lv, Z., Yuan, Y., Xu, Q., 2021. Mitochondria-related core genes and TF-miRNA-hub mrDEGs network in breast cancer. Bioscience Reports, 41.

[64] Bergmeyer, H.U., 1974. Methods of enzymatic analysis, 2nd ed. New York (NY): Academic Press.

